

Computational and experimental characterization of a pyrrolidinium-based ionic liquid for electrolyte applications

Hedieh Torabifard, Luke Reed, Matthew T. Berry, Jason E. Hein, Erik Menke, and G. Andrés Cisneros

Citation: [The Journal of Chemical Physics](#) **147**, 161731 (2017);

View online: <https://doi.org/10.1063/1.5004680>

View Table of Contents: <http://aip.scitation.org/toc/jcp/147/16>

Published by the [American Institute of Physics](#)

Articles you may be interested in

[Links between the charge model and bonded parameter force constants in biomolecular force fields](#)

The Journal of Chemical Physics **147**, 161730 (2017); 10.1063/1.4985866

[The truncated conjugate gradient \(TCG\), a non-iterative/fixed-cost strategy for computing polarization in molecular dynamics: Fast evaluation of analytical forces](#)

The Journal of Chemical Physics **147**, 161724 (2017); 10.1063/1.4985911

[Restricted lithium ion dynamics in PEO-based block copolymer electrolytes measured by high-field nuclear magnetic resonance relaxation](#)

The Journal of Chemical Physics **147**, 134902 (2017); 10.1063/1.4993614

[Intermolecular interactions in the condensed phase: Evaluation of semi-empirical quantum mechanical methods](#)

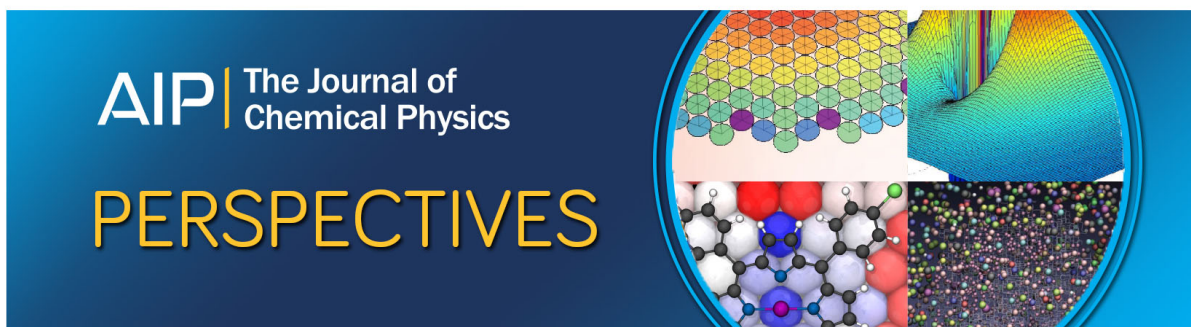
The Journal of Chemical Physics **147**, 161704 (2017); 10.1063/1.4985605

[Structure and polarization near the Li⁺ ion in ethylene and propylene carbonates](#)

The Journal of Chemical Physics **147**, 161710 (2017); 10.1063/1.4992788

[Development of reactive force fields using ab initio molecular dynamics simulation minimally biased to experimental data](#)

The Journal of Chemical Physics **147**, 161719 (2017); 10.1063/1.4985903



Computational and experimental characterization of a pyrrolidinium-based ionic liquid for electrolyte applications

Hedieh Torabifard,¹ Luke Reed,² Matthew T. Berry,³ Jason E. Hein,³ Erik Menke,² and G. Andrés Cisneros^{4,a)}

¹Department of Chemistry, Wayne State University, Detroit, Michigan 48202, USA

²Department of Chemistry and Chemical Biology, University of California-Merced, Merced, California 95343, USA

³Department of Chemistry, University of British Columbia, Vancouver, British Columbia V6T 1Z1, Canada

⁴Department of Chemistry, University of North Texas, Denton, Texas 76203, USA

(Received 1 May 2017; accepted 14 September 2017; published online 4 October 2017)

The development of Li-ion batteries for energy storage has received significant attention. The synthesis and characterization of electrolytes in these batteries are an important component of this development. Ionic liquids (ILs) have been proposed as possible electrolytes in these devices. Thus, the accurate determination of thermophysical properties for these solvents becomes important for determining their applicability as electrolytes. In this contribution, we present the synthesis and experimental/computational characterization of thermodynamic and transport properties of a pyrrolidinium based ionic liquid as a first step to investigate the possible applicability of this class of ILs for Li-ion batteries. A quantum mechanical-based force field with many-body polarizable interactions has been developed for the simulation of spirocyclic pyrrolidinium, [sPyr⁺], with BF₄⁻ and Li⁺. Molecular dynamics calculations employing intra-molecular polarization predicted larger heat of vaporization and self-diffusion coefficients and smaller densities in comparison with the model without intra-molecular polarization, indicating that the inclusion of this term can significantly effect the inter-ionic interactions. The calculated properties are in good agreement with available experimental data for similar IL pairs and isothermal titration calorimetry data for [sPyr⁺][BF₄⁻]. Published by AIP Publishing. <https://doi.org/10.1063/1.5004680>

INTRODUCTION

Lithium-ion batteries are widely used in various areas including portable electronics, electric vehicles, and aerospace applications, due to their high energy density, low self-discharge, low maintenance, and small size and weight. Lithium-ion battery technology shows great promise as power sources that can revolutionize the electric vehicles industry. Typically, organic electrolytes such as ethylene carbonate (EC) have been used in batteries; however, these types of electrolytes are volatile and flammable, raising safety concerns especially for high temperature applications. Recently, ionic liquids have been introduced as new electrolytes for lithium-ion batteries due to their unique properties. However, these electrolytes are most commonly identified as poor electrolytes in batteries.^{1–3} To address this issue, a detailed, atomic-level understanding of ion transport processes and redox stability would help improve the design of electrolyte-electrode couples in batteries. Our combined chemical and experimental approach was inspired by this principle to design a new electrolyte for Li-ion batteries.

The wide variety of cation-anion combinations make the synthesis and experimental determination of ILs properties an expensive and time-consuming process. The synthesis

of highly pure ILs places particular demands on the preparative work. Moreover, predicting which ILs are well suited for a given application remains an important pre-synthesis pursuit. To this end, computer simulations have become a useful tool to predict IL properties to aid in the discovery process.

Many structural, thermodynamic, and transport properties can be predicted by employing molecular dynamics (MD) methods.^{4–12} Most of the IL simulations to date have used non-polarizable¹³ or polarizable¹⁴ force fields with partial atomic charges. The use of point charges to describe the electrostatic interactions results in loss of accuracy in the reproduction of the Coulomb interaction due to lack of anisotropy and penetration effect at short interatomic distances.^{15,16} One possibility to improve the accuracy of the results is to employ higher order distributed multipoles.^{17,18}

Recently, some of us have developed a multipolar-polarizable force field for ILs based on the AMOEBA potential coupled with the use of distributed multipoles obtained from the Gaussian Electrostatic Model (GEM).^{19–24} Our initial tests on imidazolium-based ionic liquids have resulted in very good agreement with respect to experiment for several condensed-phase properties such as density, diffusion coefficients, heats of vaporization, and water exchange rates.^{19,22}

In this contribution, we present a combined theoretical and experimental study involving the synthesis and characterization of spirocyclic pyrrolidinium tetrafluoroborate

^{a)}Author to whom correspondence should be addressed: andres@unt.edu

[sPyr⁺][BF₄⁻]. In addition, a computational study on the properties of this IL pair with added Li is presented. The section titled Methods describes a brief overview of the parametrization details (described in detail previously^{19,21,22}) followed by a description of the experimental synthesis and characterization and the details of the MD simulations. Subsequently, the section titled Results details the results and discussion for both the experimental and theoretical characterizations of some thermodynamical and transport properties, followed by concluding remarks.

METHODS

Computational methods

Parameter determination

The determination of AMOEBA parameters for ILs has been described in detail earlier.^{19,22} Briefly, most classical force fields are comprised of bonded and non-bonded parameters. For the ions in the present study, the bonded terms were taken directly from published AMOEBA parameters without any adjustment.^{25–27} By contrast, the non-bonded terms, described by Eq. (1), have been fitted to reproduce Coulomb, polarization, and the Van der Waals energies based on QM energy decomposition analysis (EDA),

$$U_{\text{non-bonded}} = U_{\text{Coul}} + U_{\text{Pol}} + U_{\text{vdW}}. \quad (1)$$

We first calculated the total inter-molecular, Coulomb, polarization, and Van der Waals energies using quantum mechanics as a reference for fitting our parameters. Total inter-molecular energies were calculated using the counterpoise correction to take into account the basis set superposition error (BSSE)²⁸ at the MP2/6-311G(d) level for dimers. The inter-molecular polarization interactions for each pair were calculated using the restricted variational space (RVS) decomposition approach²⁹ at the HF/6-311G(d) level of theory as implemented in GAMESS.^{30,31} An in-house FORTRAN90 program that uses *ab initio* monomer electron densities was employed to calculate the Coulomb inter-molecular energies for each dimer. Finally, the Van der Waals energies were obtained by subtracting the Coulomb and polarization energies from total intermolecular energy for each dimer, as described in Eq. (2),

$$U_{\text{vdW}(\text{MP2-HF})} = U_{\text{Tot}(\text{MP2})} - (U_{\text{Coul}(\text{MP2})} + U_{\text{Pol}(\text{HF})}). \quad (2)$$

The non-bonded terms in the AMOEBA potential include polarization, Van der Waals, and Coulomb. The polarization energy is calculated by inducible atomic dipoles on each interaction (atomic) site. Here, each induced dipole is obtained by $\mu_{i,\alpha}^{\text{ind}} = \alpha_i E_{i,\alpha}$, where α is the atomic polarizability and $E_{i,\alpha}$ is the external electric field generated by both permanent multipoles and induced dipoles. The Tholé damping function^{15,32} is employed to avoid the “polarization catastrophe” at short range.

In this study, the intra-molecular polarization is also taken into account for spirocyclic pyrrolidinium.²⁷ Since spirocyclic pyrrolidinium is not a planar molecule, the changes in each ring of this molecule may change the electron density distribution

of the whole molecule. Hence, two sets of parameters have been developed: (1) One with no intra-molecular polarization for [sPyr⁺], i.e., 1 polarization group, termed 1G and (2) one with intra-molecular polarization in [sPyr⁺] where each ring and the central nitrogen atom were polarized separately, i.e., three polarizable groups (3G).

The Van der Waals potential energy is described by the buffered Halgren³³ pairwise potential [see Eq. (3)]

$$U_{\text{vdw}}(r_{ij}) = \epsilon_{ij} \left(\frac{1 + 0.07}{\left(\frac{r_{ij}}{R_{ij}^0} \right) + 0.07} \right)^7 \left(\frac{1 + 0.12}{\left(\frac{r_{ij}}{R_{ij}^0} \right)^7 + 0.12} - 2 \right), \quad (3)$$

where ϵ_{ij} is the potential well, r_{ij} is the separation distance between sites i and j , and R_{ij}^0 is the minimum energy interaction distance for sites i and j .³⁴

Finally, distributed atomic multipoles are used to describe the electrostatic (Coulomb) interactions. In this case, following our previous work, the distributed multipoles are obtained from the fitting of quantum mechanical (QM) electronic density via the Gaussian Electrostatic Model (GEM) fitting procedure. Briefly, GEM is a potential that employs Hermite Gaussians to calculate each term of the QM EDA. Furthermore, the use of Hermite Gaussians results in a direct relation with point multipoles which enables the calculation of robust and strictly convergent distributed multipoles, termed GEM-distributed multipoles or GEM-DM.^{23,24} GEM-DM up to quadrupoles on each atom for each monomer (in the optimized geometry) was obtained using relaxed electronic densities for the monomers calculated at the MP2/6-311G(d) level with the GEM-fit program.²¹

The accuracy of the fitted GEM density is tested by comparing the intermolecular Coulomb interaction calculated with GEM, with its QM counterpart from the relaxed QM densities. In our previous work,¹⁹ the GEM densities were fitted as a function of the change in a 1D scan along the distance between the dimers. This leads to less accurate sampling for all the possible interactions in the bulk. Hence, in this study, our fitting methodology has been modified, and instead, for this work, the GEM densities have been fitted using a series of random dimers²² (see the section titled Results).

The optimization of the GEM densities and associated distributed multipoles for sPyr⁺ and BF₄⁻ has been optimized separately by calculating the intermolecular Coulomb interaction of each ion with a single water molecule. The GEM densities and distributed multipoles for the water fragment have been previously fitted and reported in our previous paper.²⁰ Once the densities and multipoles for the ions were optimized, the intermolecular interaction between the cation and anion was used to validate the fit (see below). The values for the optimized multipoles for spirocyclic pyrrolidinium and tetrafluoroborate are reported in the supplementary material.

One additional advantage of performing the RVS calculations for the random dimers is that this provides a QM reference for each non-bonded term in the intermolecular interaction. Thus, the polarization and Van der Waals terms are also optimized by comparing to their RVS counterparts as described above.^{20,35} Once all parameters for the new

molecules have been fitted by comparing with QM data, the total intermolecular energies for the [sPyr⁺][BF₄⁻] dimers are compared with counterpoise corrected total intermolecular interactions obtained with the Gaussian09 package.³⁶ The inter-molecular, Coulomb, polarization, Van der Waals, and total energies using the optimized parameters for a series of random dimers of [sPyr⁺][BF₄⁻] were obtained with the analyze module available in TINKER.³⁷

MD simulation details

MD simulations were carried out with pmemd.gem, an in-house development version of pmemd from the AMBER suite,³⁸ using the AMOEBA/GEM-DM force field. The MD simulations were performed using an orthorhombic simulation cell with periodic boundary conditions. The calculated system included 216 dimers. For the Li doped system, 22 spirocyclic pyrrolidinium cations were replaced with Li⁺ ions to make a mixture of 10% Li ion doped into the IL. All systems were minimized with 1000 conjugate steps, and heated up to 600 K with 20 000 steps to make sure they are in liquid phase. Subsequently, all systems were cooled down with 50 000 steps to the desired temperatures. The productions were carried out in the NPT ensemble with an integration time step of 1 fs. Long-range electrostatic effects were computed employing the smooth particle mesh Ewald method³⁹⁻⁴¹ with an 8 Å direct cutoff (also used for VdW), a B-spline order of 5, an Ewald exponent of 0.45, and a grid size of 48 points. Sampling trajectories for neat IL were generated for 10 ns and for Li salt doped mixture for 20 ns.

Calculated properties from the generated ensembles include density (ρ), heat of vaporization (ΔH_{vap}), diffusion coefficient (D_{\pm}), and radial distribution functions (RDFs). The density and volume data are obtained directly from MD outputs. The heat of vaporization, which is an estimation of the inter-molecular interaction strength of ionic pairs, is calculated using Eq. (4),

$$\Delta H_{vap} = \Delta E + \Delta nRT, \quad (4)$$

where ΔE is the difference between potential energy in the gas and liquid phase.

The enthalpy of vaporization is calculated as the energy required to take an ionic pair from the liquid to the gas phase. Gas phase simulations were carried out using stochastic molecular dynamics simulations of a single ionic pair at each temperature using the dynamic module in TINKER.³⁷

The self-diffusion coefficient is another liquid property that reflects the quality of the force fields implemented in MD simulations. The mobility of ionic species depends on many parameters including the geometric structure, ion size, charge delocalization, and strength of intermolecular interactions. The ion self-diffusion coefficients were calculated using Einstein's relation

$$D_{\pm} = \lim_{t \rightarrow \infty} \frac{\langle \text{MSD}(t)_{\pm} \rangle}{6t}, \quad (5)$$

where $\langle \text{MSD}(t) \rangle$ is the mean squared displacement of the molecule's center of mass and t is the time. The mean squared displacement [MSD(t)] in the diffusive regime was calculated from the production trajectories.

Liquid structures of ionic liquids are usually compared to X's-ray scattering¹¹ or neutron diffraction experimental data.⁴² In particular, inter-ionic correlations are well described by radial distribution functions and can be compared with the structural factor $S(Q)$ obtained from neutron diffraction.⁴² Radial distribution functions (RDFs) were calculated at different temperatures for cation-cation, anion-anion, and cation-anion pairs.

Experimental methods

Synthesis and characterization of [sPyr⁺][BF₄⁻]

1,4-dibromobutane (3.4 g, 15.75 mmol) was dissolved in acetonitrile (15 ml) in a 50 ml round-bottom flask, to which K₂CO₃ (2.4 g, 17.37 mmol) was added. Pyrrolidine (1.3 ml, 15.57 mmol) was added via a syringe, and the mixture was heated at 353 K overnight. The reaction mixture was cooled to room temperature, and solids were filtered on a Celite pad into a 100 ml round-bottom flask. NaBF₄ (1.7 g, 15.48 mmol) was added to the filtrate, and the mixture was stirred overnight. Solids were filtered on a pad of Celite and the solvent was removed *in vacuo*. The crude residue was reconstituted in a minimum volume of acetonitrile, and the product was precipitated by the addition of diethyl ether. The solids were collected by vacuum filtration to yield the product (2.66 g, 79% yield) as a deliquescent off-white solid. Chemicals and solvents were purchased from Sigma-Aldrich and Fisher Scientific and used without any further purification.

The characterization of the IL pair was performed via NMR spectroscopy to confirm the structure of the newly synthesized salt. ¹H NMR, ¹³C NMR, and ¹⁹F NMR spectra were recorded on a Bruker AV400sp spectrometer at 298 K at field strengths of 400 MHz, 100 MHz, and 375 MHz, respectively. The NMR data are presented in the section titled Results.

After synthesis of the IL, differential scanning calorimetry (DSC) was performed on the BF₄⁻ compound with a Perkin Elmer Jade DSC. Approximately 2 mg of the BF₄⁻ compound was placed in aluminum DSC pans, and the sample was heated at 2 K/min to 473 K for the BF₄⁻ compound and then cooled to 298 K at 2 K/min. The DSC results are presented in the section titled Results.

RESULTS

Parameter fitting

In order to fit the multipoles for each molecular fragment, the same methodology implemented for nonionic compounds was used as described previously.^{20,22} We randomly generated thirty dimers of cation-water and twenty dimers of anion-water and calculated the Coulomb energies for each dimer. The Coulomb energies are calculated with GEM, GEM-DM, and QM (from the relaxed QM densities of the monomers). We have previously shown that fitting the GEM density and distributed multipoles of ions using ion-water dimers results in accurate and transferable multipoles.²² The multipoles for [sPyr⁺] and [BF₄⁻] are presented in Tables S1–S3 of the supplementary material.

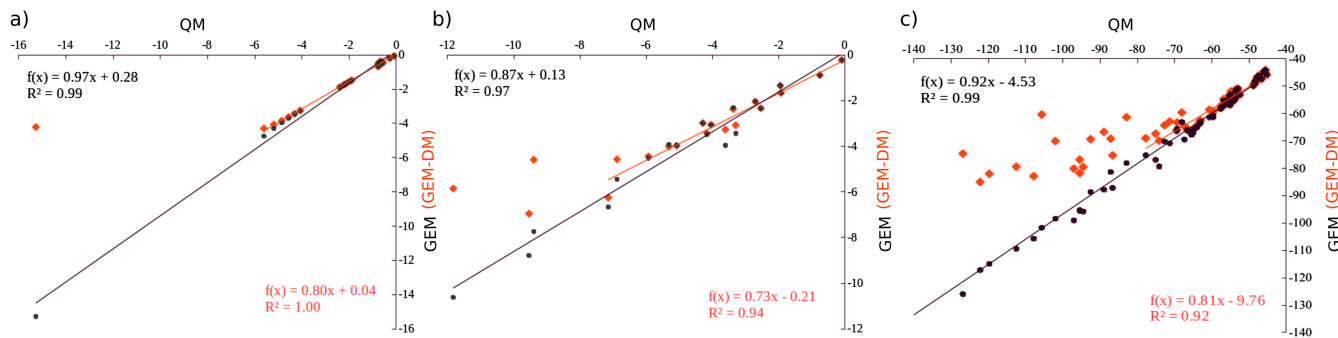


FIG. 1. Coulomb energies calculated for (a) cation–water and (b) anion–water (c) $[\text{sPyr}^+][\text{BF}_4^-]$ dimers using GEM (black) and GEM–DM (red) compared with QM. The Coulomb energies smaller than -8 kcal/mol for cation/anion–water dimers using GEM, and -80 kcal/mol for $[\text{sPyr}^+][\text{BF}_4^-]$ dimers using GEM–DM are not included in the linear fitting to exclude dimers with high penetration errors.

Figure 1 shows the comparison of Coulomb energies calculated for spirocyclic pyrrolidinium–water, tetrafluoroborate–water and $[\text{sPyr}^+][\text{BF}_4^-]$ dimers using GEM and GEM–DM with full QM. As expected, the Coulomb energies calculated with the full GEM densities are well correlated with the QM reference energies. Conversely, this correlation decreases when multipoles (GEM–DM) are employed due to the penetration error. The excellent correlation in Coulomb energies for $[\text{sPyr}^+][\text{BF}_4^-]$ dimers using GEM [Fig. 1(c)] indicates that although the electron densities and multipoles for each ion are fitted using water–ion dimers, they provide a very good description of Coulomb interactions for the ionic liquid dimers. The comparison of Coulomb energies calculated for cation–cation and anion–anion dimers using GEM, GEM–DM, and QM is presented in Fig. S1 of the [supplementary material](#).

Once the multipoles for the ions had been obtained, intermolecular interaction energies were determined for 77 random dimers of $[\text{sPyr}^+][\text{BF}_4^-]$ using QM EDA as a reference and the new force field using both sets of parameters [with (3G) and without (1G) intra-molecular polarization for $[\text{sPyr}^+]$]. The total interaction energy in the gas phase was calculated at the MP2(full)/6-311G(d) level of theory. The total intermolecular interaction energies were decomposed using the RVS²⁹ decomposition analysis. The resulting inter-molecular potential along with the corresponding energy components using 1 and 3 polarizable groups (1G–3G) is given in Fig. 2 for the $[\text{sPyr}^+][\text{BF}_4^-]$ pair. The correlation of Coulomb energy in QM/MM improves significantly by excluding the dimers with very close intermolecular distances in curve fitting (Fig. S2 of the [supplementary material](#)). However, since the correlation between QM and MM energies for both sets of force fields is very similar, therefore, MD simulations were performed with both sets of force fields to find out which one describes the behavior of the system better and is in better agreement with experimental data. Figures S3 and S4 of the [supplementary material](#) show the inter-molecular potential with corresponding energy components for $[\text{sPyr}^+][\text{sPyr}^+]$ and $[\text{BF}_4^-][\text{BF}_4^-]$ dimers.

MD simulations

The MD simulations have been performed for neat IL ($[\text{sPyr}^+][\text{BF}_4^-]$) and the mixture ([10% $\text{Li}^+][\text{BF}_4^-]$ –[90%

$[\text{sPyr}^+][\text{BF}_4^-]$]) with and without intra-molecular polarization (3G and 1G) at $T = 300$ – 500 K in 50 K increments. Two independent simulations have been performed with the 3G parameter set in neat IL for all temperatures and in the mixture at 500 K. Total and potential energies calculated for each test with 3G parameter set at 300–500 K are presented in Figures S5 and S6 of the [supplementary material](#).

Density

The density of neat $[\text{sPyr}^+][\text{BF}_4^-]$ was calculated for a range of temperatures between 300 and 500 K as shown in Fig. 3 using both parameter sets (3G and 1G). The calculated densities are 4%–8% smaller when the intra-molecular polarization is included in the force field (3G parameter set). Overall, the densities calculated using 1G and 3G parameter sets decrease by 12.7% and 16.1%, respectively, from 300 K to 500 K. This change is not linear with respect to the increase in temperature. A case in point, the largest density change occurs within 400–450 K, where the calculated ρ decreases by 5.2% (3.4%) for the 3G (1G) sets, respectively. The density and volume using the parameters with 3 polarizable groups at 400 K are 1.14 g/cm^3 and 324.70 \AA^3 , respectively, compared with 1.09 g/cm^3 and 308.12 \AA^3 at 450 K. The densities (volume) at 400 K and 450 K obtained with the other parameter set (1G) are 1.19 g/cm^3 (297.45 \AA^3) and 1.15 g/cm^3 (303.31 \AA^3). There are no experimental data available for this particular IL pair for the calculated properties. However, comparison is possible between our results with simulated or experimental data for 1-N-butyl-1-methyl-pyrrolidinium tetrafluoroborate ($[\text{Pyr}_{14}^+][\text{BF}_4^-]$), 1-N-propyl-1-methyl-pyrrolidinium tetrafluoroborate ($[\text{Pyr}_{13}^+][\text{BF}_4^-]$), or other similar cations.^{43–45} Chaban *et al.* calculated a series of properties for 1-N-butyl-1-methyl-pyrrolidinium tetrafluoroborate ($[\text{Pyr}_{14}^+][\text{BF}_4^-]$) within 298–353 K.⁴³ The density calculated within these temperature is around 1.05 g/cm^3 , which is in the range of the density we calculated at 300–350 K using the 3G parameter set (1.20 g/cm^3 at 300K, 1.18 at 350 K). Experimental density for 1-N-butyl-1-methoxymethyl-pyrrolidinium tetrafluoroborate and 1-N-butyl-1-methoxylethyl-pyrrolidinium tetrafluoroborate at 298 K is 1.25 g/cm^3 and 1.24 g/cm^3 , respectively.⁴⁵

To further investigate the possibility of the application of these newly designed electrolytes in Li-ion batteries, a system

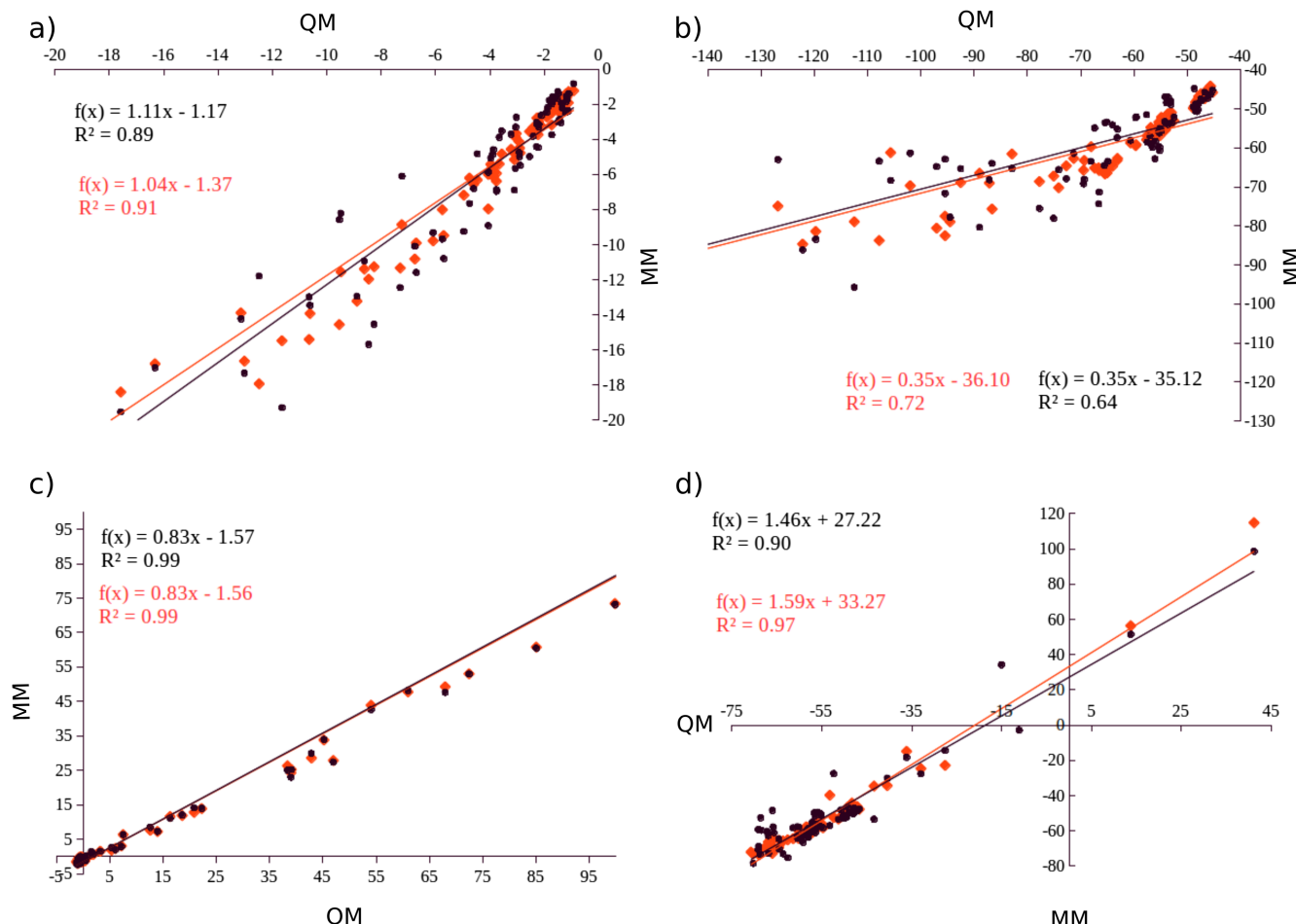


FIG. 2. (a) Polarization, (b) Coulomb, (c) vdW, and (d) total energies calculated for $[\text{sPyr}^+][\text{BF}_4^-]$ dimers in QM and MM with 3 polarizable groups (black) and 1 polarizable group (red). The new curve fitting for Coulomb energies is presented in Fig. S4.

was created where 10% Li ions were doped in the ionic liquid simulation box to observe the changes in thermodynamic properties of our system. Overall, the density of the mixture calculated with both parameter sets is ~2%-4% higher than the density in the neat IL for all the temperatures (Fig. 3). The larger density value for the mixture compared to the neat

IL is consistent with the reported densities for neat and mixture ionic liquids in the literature.^{44,46-48} For instance, Borodin *et al.* reported that the density of [25% Li^+][75% mmipy $^+$] $[\text{TFSI}^-]$ increases by 5% compared to neat [mmipy $^+$] $[\text{TFSI}^-]$.⁴⁴ Similar to neat IL, a large change in density (5.4% and 3.1% for 3G and 1G, respectively) between 400 and 450 is observed for the mixture. The density and volume using the parameters with 3 polarizable groups at 400 K are 1.18 g/cm^3 and 282.84 \AA^3 , respectively, compared to 1.13 g/cm^3 and 296.31 \AA^3 at 450 K. The densities (volume) at 400 K and 450 K obtained with the non-polarizable force field are 1.21 g/cm^3 (275.06 \AA^3) and 1.18 g/cm^3 (282.31 \AA^3).

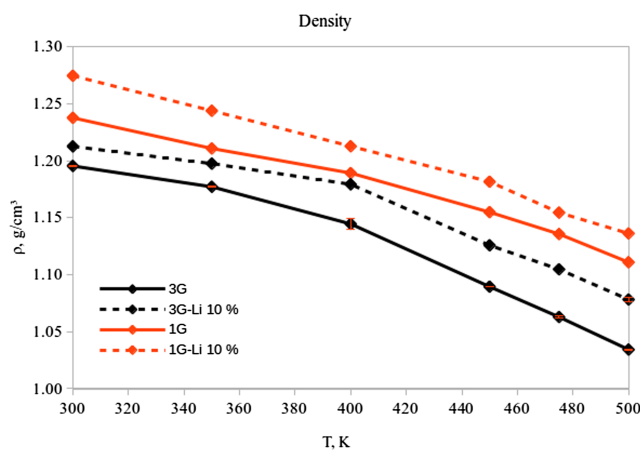


FIG. 3. Densities (ρ) calculated for $[\text{sPyr}^+][\text{BF}_4^-]$ with 1 and 3 polarizable groups for 300–500 K.

Enthalpy of vaporization

The heat of vaporization energies were calculated at $T = 300$ – 500 K with both sets of parameters and are reported in Table I. Gas phase energies presented in Table I are calculated for a single dimer using dynamic module in TINKER³⁷ and bulk energies are obtained directly from MD simulations in different temperatures.

As seen in Table I, the heat of vaporization values obtained with the 3G parameter set are almost double as the values

TABLE I. Heat of vaporization for $[s\text{Pyr}^+][\text{BF}_4^-]$ between 300 and 500 K. The values are in kcal/mol. The error bars are calculated from heat of vaporization values of each independent simulation. The simulation with the 3G (1G) model has been performed two times (once).

T	AMOEBA/GEM-DM (1G)			AMOEBA/GEM-DM (3G)		
	Gas	Bulk	ΔH_{vap}	Gas	Bulk	ΔH_{vap}
300	-69.02	-104.21	35.79	-110.04	-180.68 ± 0.15	71.24 ± 0.15
350	-64.94	-99.14	34.90	-106.53	-176.47 ± 0.34	70.64 ± 0.34
400	-60.42	-93.62	34.00	-101.42	-172.01 ± 0.18	71.39 ± 0.18
450	-55.91	-87.65	31.83	-97.16	-166.13 ± 0.01	70.17 ± 0.67
475	-54.91	-84.94	30.97	-95.57	-163.62 ± 0.01	68.99 ± 0.01
500	-52.22	-81.98	30.76	-92.84	-160.74 ± 0.01	68.89 ± 0.01

obtained with the 1G force field. These results suggest that taking the intra-molecular polarization into account results in stronger inter-ionic interactions in comparison with the model without intra-molecular polarization. The experimental and computational heat of vaporization has been reported between 30 and 50 kcal/mol for various pyrrolidinium-based ionic liquids, such as $[\text{C}_{n1}\text{ Pyr}^+][\text{NTf}_2^-]$ at 298 K,⁴⁹ $[\text{Pyr}_{14}^+]$, $[\text{BF}_4^-]$ at 298–353 K.⁴³ It has been shown that the heat of vaporization increases as the size of the ions increases.^{43,49} Therefore, it is expected to obtain larger heat of vaporization in $[\text{sPyr}^+][\text{BF}_4^-]$ due to the large size of the cation.

Diffusion coefficients

Self-diffusion coefficients for $[\text{sPyr}^+][\text{BF}_4^-]$ using AMOEBA/GEM-DM at T = 300–500 K are shown in Fig. 4. Generally, as the temperature increases, the molecules move faster and consequently the self-diffusion coefficients increase. However, the self-diffusion coefficient calculated by employing the 1G parameter set does not change significantly with increasing temperature. D_{\pm} increased by 5.6% between 300 and 500 K. By contrast, the inclusion of intra-molecular polarization (3G parameter set) results in a large increase of D_{\pm} (65.1%) between 300 and 500 K. This suggests that the inclusion of a better description of many body interactions speeds up the ion diffusion for this system.

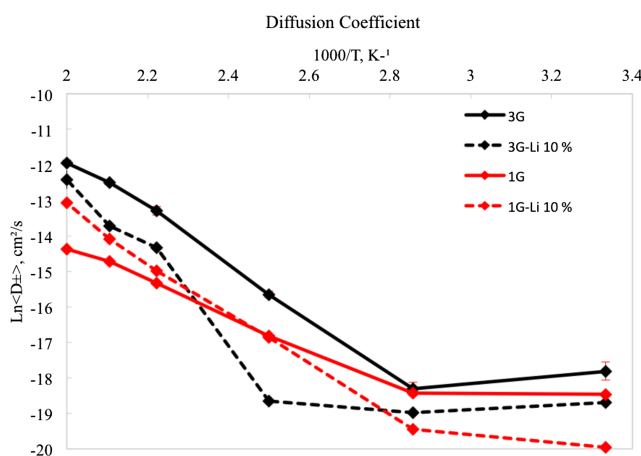


FIG. 4. Diffusion coefficients (D_{pm}) calculated for $[\text{sPyr}^+][\text{BF}_4^-]$ with 1 and 3 polarizable groups for 300–500 K.

The self-diffusion coefficient for $[\text{sPyr}^+][\text{BF}_4^-]$ using the 3G parameter set shows negligible change within 300–400 K (less than 1.5%). From 400 K to 450 K, an increase in D_{\pm} of 15.3% is observed. The average diffusion coefficients for anion and cations (D_{\pm}) at 400 K is $0.02 \times 10^{-5} \pm 0.002 \text{ cm}^2 \text{ s}^{-1}$ and at 450 K is $0.17 \times 10^{-5} \pm 0.02 \text{ cm}^2 \text{ s}^{-1}$. The diffusion coefficient changes are almost negligible (1.7%) when intra-molecular polarization is not taken into account (1G parameter set). Experimental diffusion for $[\text{Pyr}_{13}^+][\text{BF}_4^-]$ has been reported to be $0.2 \times 10^{-5} \text{ cm}^2 \text{ s}^{-1}$ at 340 K.⁴³ Chaban *et al.* calculated $0.06 \times 10^{-5} \text{ cm}^2 \text{ s}^{-1}$ for diffusion coefficient of $[\text{Pyr}_{14}^+][\text{BF}_4^-]$ at 338 K.⁴³ These results are consistent with the calculated self-diffusion coefficients for $[\text{sPyr}^+][\text{BF}_4^-]$ considering that the larger size of the cation should result in slower diffusion.

The average self-diffusion coefficients for [10% Li⁺] $[\text{BF}_4^-]$ -[90% sPyr⁺] $[\text{BF}_4^-]$ at T = 300–500 K using 1 and 3 polarizable groups are presented in Fig. 4. The self-diffusion coefficients for each ion in the neat IL and the mixture using 1G and 3G force fields are shown in Figs. S7 and S8 of the [supplementary material](#). The ion diffusion in the mixture is very similar to the neat IL at lower temperatures (300–400K) using both parameter sets (less than 0.1% and 2.0% using 1G and 3G parameter sets, respectively). However, ions diffuse slower in the Li-doped mixture in comparison with neat IL at higher temperatures using the 3G parameter set. The self-diffusion coefficients at 450 K, 475 K, and 500 K decreased by 9.9%, 19.5%, and 22.2%, respectively, compared to neat IL. This could be due to stronger inter-ionic interactions between the Li ions and the anions using the 3G parameter set.

Conversely, the ions diffuse faster in the 10% Li⁺/IL mixture than in the neat IL when the 1G parameter set is employed. The diffusion is observed to increase by 0.6%, 5.2%, and 10.9% at 450 K, 475 K, and 500 K, respectively, likely due to the reduced accuracy in the description of the many-body effects. In particular, because of the inability of the 1G model to describe the change in the charge density distributions due to a change in the internal structure of the sPyr. At higher temperatures, the sPyr molecules experience larger changes in internal structure due to the flexibility of the two rings. However, only the 3G set is able to describe the change in intra-molecular polarization. Indeed, it is observed that for the systems simulated with the 3G parameter set, the average polarization energy becomes more attractive by around 2%

going from 450 K to 500 K. Conversely, the average polarization energy is observed to decrease by around 10% with increasing temperature for the 1G simulated systems for the same temperature range. Several studies show that the self-diffusion coefficients decrease by adding Li ions to the neat ionic liquids due to strong interaction between Li ions and anions.^{47,48,50} Thus, the self-diffusion calculated with the 3G parameter set in our study is in better agreement with the available experimental/computational results. These results underscore the importance for the inclusion of intra-molecular polarization for flexible molecules.

To further probe the dynamical properties of these systems, we studied the mean square displacement (MSD). Figure S9 of the [supplementary material](#) shows the $\langle \text{MSD} \rangle$ as a function of time which indicates the mobility differences at different temperatures using the 1G and 3G models in neat IL and the mixture. In the 3G model, for both the neat IL and the mixture, the MSD starts initially from a ballistic regime ($\propto t^2$) and finally reaches the diffusive regime ($\propto t$). This behaviour is observed at $T = 450\text{--}500$ K, although the slope of the MSD decreases as T is lowered. At lower temperatures, the slope of the MSD decreases significantly. At $T = 300\text{--}350$ K, the MSD is observed to remain almost constant with time, indicating that the mobility of the systems is significantly reduced at these temperatures compared to those at higher temperatures. A similar behaviour is observed for the 1G model. Figure S10 of the [supplementary material](#) compares the MSD plots for all models at different temperatures.

Radial distribution function (RDF) and structural analysis

The RDF for the anion–anion (B–B), anion–cation (B–N), and cation–cation (N–N) pairs for the neat IL in all the tested temperatures (300–500 K) using the 1G and 3G parameter sets is depicted in Fig. 5 and Fig. S11 of the [supplementary material](#). A small peak at 4 Å is observed for the B–B RDF at 300, 350, and 400 K, which is correlated to a close distance between $[\text{BF}_4^-]$ ions at these temperatures using the 3G parameter set. This peak vanishes at higher temperatures. Similarly, a plateau for the cation–cation (N–N) RDF is observed around 9.5 Å for the 300–400 K range but missing at higher temperatures. The small peak at 4 Å for the B–B and plateau for the N–N RDF are not observed using the 1G parameter set. The N–B RDF shows two distinct peaks around 5 Å with $g(r)$ of ~5.5 and 2.5 using the 3G parameter set, while it shows a single peak with a small shoulder with $g(r)$ of 3.0 using the 1G force field. These results provide further support that the inclusion of intra-molecular polarization provides stronger inter ionic interactions in this system.

The overlay of the RDFs calculated with 1 and 3 polarizable groups for the mixture is presented in the SI (Figs. S12 and S13 of the [supplementary material](#)). The small peak at 4 Å which was only observed for B–B RDF at low temperatures using 3G parameters is now distinguishable for all temperatures in both B–B RDF using 1G and 3G force fields. Similar results are obtained for N–B RDF using 1G and 3G

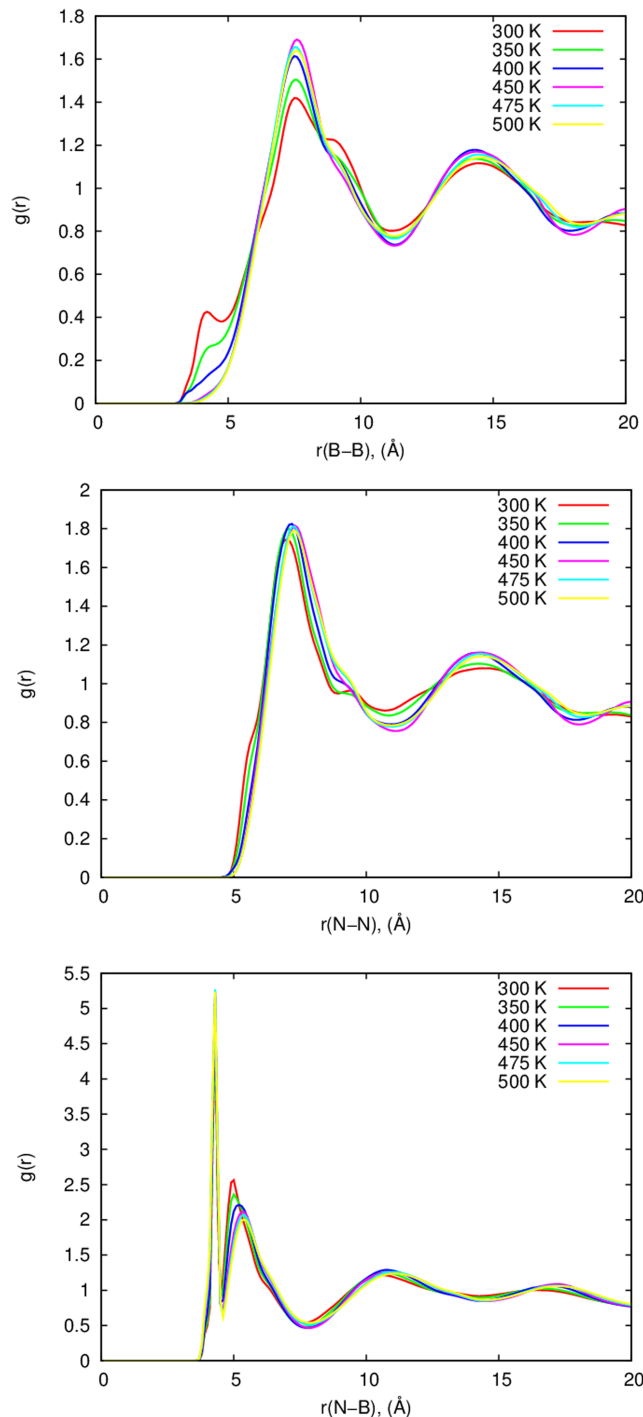


FIG. 5. Radial distribution function for $[\text{sPyr}^+][\text{BF}_4^-]$ with three polarizable groups (3G).

parameter sets in the neat IL and the mixture. The Li–N/B RDFs also confirm that the inclusion of intra-molecular polarization could change the structure of our system. For instance, the Li–B RDF using 3G parameter set shows three distinct peaks less than 5 Å, while only one peak is observed using the 1G parameter set. Conversely, the Li–N RDF for the 3G force field shows a single peak at 4 Å with $g(r)$ of 7, while there are 3 peaks with $g(r)$ less than 2 for 1G force field. Further studies are under way to investigate the Li ion behavior in this mixture at different temperatures.

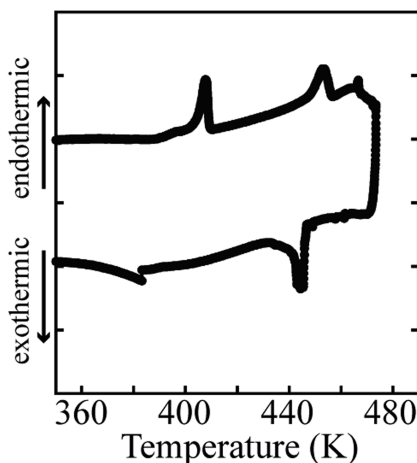


FIG. 6. Experimental DSC for $[\text{sPyr}^+]\text{[BF}_4^-]$ at $T = 360\text{--}480\text{ K}$.

NMR spectroscopy for $[\text{sPyr}^+]\text{[BF}_4^-]$

After having successfully established the synthesis of spirocyclic pyrrolidinium tetrafluoroborate as described in the section titled Methods, the structure of the newly synthesized IL was confirmed by $^1\text{H NMR}$, $^{13}\text{C NMR}$, and $^{19}\text{F NMR}$. The NMR spectroscopy data for salt are: $^1\text{H NMR}$ (400 MHz, CDCl_3) δ 4.13–3.33 (m, 8H), 2.29 (s, 8H); $^{13}\text{C NMR}$ (100 MHz, CDCl_3) δ 62.92, 22.12; $^{19}\text{F NMR}$ (375 MHz, CDCl_3) δ –151.81.

DSC analysis for $[\text{sPyr}^+]\text{[BF}_4^-]$

Following the interesting results obtained from the computational simulations, differential scanning calorimetry was performed on the synthesized $[\text{sPyr}^+]\text{[BF}_4^-]$. Figure 6 shows a typical DSC run from 360 K to 480 K for the BF_4^- compound. The DSC for the BF_4^- compound shows that the melting temperature is about 448 K, and an enthalpy of fusion of 181 J/g, and a crystallization onset of 446 K and an enthalpy of crystallization of 350 J/g. However, examination of the DSC for the BF_4^- compound reveals extra peaks, suggesting the presence of impurities in the compound making the enthalpy measurements unreliable.

DISCUSSION

A significant change is observed in the calculated density, heat of vaporization, self-diffusion coefficient, and RDF for $[\text{sPyr}^+]\text{[BF}_4^-]$ within the 400–450 K range, especially when intra-molecular polarization is taken into account. Further, structural analysis shows that the disorder degree of the neat IL increases at 450 K compared to the structure at 400 K. This is also observed by additional features in the anion-anion and cation–cation RDFs at low temperatures (below the MP). The difference in these structures could explain the significant changes observed within these temperatures for the MD-calculated properties such as density and diffusion coefficient. Although we are not able to simulate the phase transition by MD simulation, the dramatic change in MD-derived properties within 400–450 K is consistent with the experimental data indicating that the melting point (phase transition from solid to liquid) of this system is about 448 K.

In addition, our results strikingly show that the inclusion of intra-molecular polarization results in stronger inter-ionic interaction and shows the properties change at 400 K accurately due to accurate description of non-bonded interactions.

The addition of Li ions into the neat IL increases the density using both parameter sets, while it shows different behaviour for self-diffusion coefficients using each of the parameter sets. The self-diffusion coefficients calculated using 3G parameter set decrease at higher temperature in the mixture compared to the neat IL. This is consistent with the available experimental/computational results for comparison of neat IL and Li-doped mixtures. Conversely, the 1G parameter set shows largest self-diffusion coefficients in the mixture in respect to the neat IL.

CONCLUSIONS

The synthesis, computational and experimental characterization of spirocyclic pyrrolidinium tetrafluoroborate has been explored as an initial step toward its evaluation as an electrolyte in Li-ion batteries. AMOEBA parameters have been developed based on the QM reference data and employed to calculate several thermodynamic properties including ρ , ΔH_{vap} , and D for a range of temperatures. Our results suggest a significant change in thermodynamic and transport properties in the 400–450 K range. Experimental synthesis of the $[\text{sPyr}^+]\text{[BF}_4^-]$ and DSC characterization shows that the melting point is around 448 K. Our results for the mixture show higher density and slower diffusion than neat IL at all temperature except the temperatures between 400 and 450 K.

SUPPLEMENTARY MATERIAL

See [supplementary material](#) for interaction energies for dimers, total and potential energy plots for all systems, diffusion plots, and distributed multipoles for $[\text{sPyr}]$ (1G and 3G).

ACKNOWLEDGMENTS

This work was supported by Wayne State University. Computing time from Wayne State's C&IT is gratefully acknowledged.

- ¹M. Armand and J.-M. Tarascon, “Building better batteries,” *Nature* **451**, 652–657 (2008).
- ²E. Markevich, V. Baranchugov, and D. Aurbach, “On the possibility of using ionic liquids as electrolyte solutions for rechargeable 5V Li ion batteries,” *Electrochim. Commun.* **8**, 1331–1334 (2006).
- ³L. Zhao, Y.-S. Hu, H. Li, Z. Wang, and L. Chen, “Porous $\text{Li}_4\text{Ti}_5\text{O}_{12}$ coated with N-doped carbon from ionic liquids for Li-ion batteries,” *Adv. Mater.* **23**, 1385–1388 (2011).
- ⁴J. N. Canongia Lopes, J. Deschamps, and A. A. Pádua, “Modeling ionic liquids using a systematic all-atom force field,” *J. Phys. Chem. B* **108**, 2038–2047 (2004).
- ⁵J. N. Canongia Lopes and A. A. Pádua, “Molecular force field for ionic liquids composed of triflate or bis(triflylimide) anions,” *J. Phys. Chem. B* **108**, 16893–16898 (2004).
- ⁶C. Cadena and E. J. Maginn, “Molecular simulation study of some thermo-physical and transport properties of triazolium-based ionic liquids,” *J. Phys. Chem. B* **110**, 18026–18039 (2006).

- ⁷T. I. Morrow and E. J. Maginn, "Molecular dynamics study of the ionic liquid 1-n-butyl-3-methylimidazolium hexafluorophosphate," *J. Phys. Chem. B* **106**, 12807–12813 (2002).
- ⁸J. B. Hooper, O. N. Starovoytov, O. Borodin, D. Bedrov, and G. D. Smith, "Molecular dynamics simulation studies of the influence of imidazolium structure on the properties of imidazolium/azide ionic liquids," *J. Chem. Phys.* **136**, 194506 (2012).
- ⁹O. Borodin, G. D. Smith, and W. Henderson, "Li⁺ cation environment, transport, and mechanical properties of the LiTFSI doped *N*-methyl-*N*-alkylpyrrolidinium⁺TFSI[−] ionic liquids," *J. Phys. Chem. B* **110**, 16879–16886 (2006).
- ¹⁰M. Bühl, A. Chaumont, R. Schurhammer, and G. Wipff, "Ab initio molecular dynamics of liquid 1, 3-dimethylimidazolium chloride," *J. Phys. Chem. B* **109**, 18591–18599 (2005).
- ¹¹J. de Andrade, E. S. Böes, and H. Stassen, "Computational study of room temperature molten salts composed by 1-alkyl-3-methylimidazolium cations force-field proposal and validation," *J. Phys. Chem. B* **106**, 13344–13351 (2002).
- ¹²C. Y. Son, J. G. McDaniel, J. R. Schmidt, Q. Cui, and A. Yethiraj, "First principles united atom force field for the ionic liquid [BMIM]⁺[BF₄[−]] : An alternative to charge scaling," *J. Phys. Chem. B* **120**, 3560 (2016).
- ¹³N. A. McDonald and W. L. Jorgensen, "Development of an all-atom force field for heterocycles. Properties of liquid pyrrole, furan, diazoles, and oxazoles," *J. Phys. Chem. B* **102**, 8049–8059 (1998).
- ¹⁴O. Borodin, "Polarizable force field development and molecular dynamics simulations of ionic liquids," *J. Phys. Chem. B* **113**, 11463–11478 (2009).
- ¹⁵A. Stone, "Distributed multipole analysis, or how to describe a molecular charge distribution," *Chem. Phys. Lett.* **83**, 233–239 (1981).
- ¹⁶M. A. Freitag, M. S. Gordon, J. H. Jensen, and W. J. Stevens, "Evaluation of charge penetration between distributed multipolar expansions," *J. Chem. Phys.* **112**, 7300–7306 (2000).
- ¹⁷D. Kosov and P. Popelier, "Atomic partitioning of molecular electrostatic potentials," *J. Phys. Chem. A* **104**, 7339–7345 (2000).
- ¹⁸P. Popelier, L. Joubert, and D. Kosov, "Convergence of the electrostatic interaction based on topological atoms," *J. Phys. Chem. A* **105**, 8254–8261 (2001).
- ¹⁹O. N. Starovoytov, H. Torabifard, and G. A. Cisneros, "Development of amoeba force field for 1, 3-dimethylimidazolium based ionic liquids," *J. Phys. Chem. B* **118**, 7156–7166 (2014).
- ²⁰H. Torabifard, O. N. Starovoytov, P. Ren, and G. A. Cisneros, "Development of an AMOEBA water model using GEM distributed multipoles," *Theor. Chem. Acc.* **134**, 1–10 (2015).
- ²¹G. A. Cisneros, "Application of Gaussian electrostatic model (GEM) distributed multipoles in the AMOEBA force field," *J. Chem. Theory Comput.* **8**, 5072–5080 (2012).
- ²²Y.-J. Tu, M. J. Allen, and G. A. Cisneros, "Simulations of the water exchange dynamics of lanthanide ions in 1-ethyl-3-methylimidazolium ethyl sulfate ([EMI][EtSO₄]) and water," *Phys. Chem. Chem. Phys.* **18**, 30323–30333 (2016).
- ²³G. A. Cisneros, D. Elking, J.-P. Piquemal, and T. A. Darden, "Numerical fitting of molecular properties to Hermite Gaussians," *J. Phys. Chem. A* **111**, 12049 (2007).
- ²⁴G. A. Cisneros, J.-P. Piquemal, and T. A. Darden, "Generalization of the Gaussian electrostatic model: Extension to arbitrary angular momentum, distributed multipoles, and speedup with reciprocal space methods," *J. Chem. Phys.* **125**, 184101 (2006).
- ²⁵P. Ren and J. W. Ponder, "Polarizable atomic multipole water model for molecular mechanics simulation," *J. Phys. Chem. B* **107**, 5933–5947 (2003).
- ²⁶P. Ren and J. W. Ponder, "Consistent treatment of inter-and intramolecular polarization in molecular mechanics calculations," *J. Comput. Chem.* **23**, 1497–1506 (2002).
- ²⁷P. Ren, C. Wu, and J. W. Ponder, "Polarizable atomic multipole-based molecular mechanics for organic molecules," *J. Chem. Theory Comput.* **7**, 3143–3161 (2011).
- ²⁸H. Jansen and P. Ros, "Non-empirical molecular orbital calculations on the protonation of carbon monoxide," *Chem. Phys. Lett.* **3**, 140–143 (1969).
- ²⁹W. J. Stevens and W. H. Fink, "Frozen fragment reduced variational space analysis of hydrogen bonding interactions. Application to the water dimer," *Chem. Phys. Lett.* **139**, 15–22 (1987).
- ³⁰M. Schmidt, K. Baldridge, J. Boatz, S. Elbert, M. Gordon, J. Jensen, S. Koseki, N. Matsunaga, K. Nguyen, S. Su *et al.*, "General atomic and molecular electronic structure system," *J. Comput. Chem.* **14**, 1347–1363 (1993).
- ³¹M. S. Gordon and M. W. Schmidt, "Advances in electronic structure theory: GAMESS a decade later," in *Theory and Applications of Computational Chemistry*, edited by C. E. Dykstra, G. Frenking, K. S. Kim, and G. E. Scuseria (Elsevier, 2005), Chap. 41, pp. 1167–1189.
- ³²B. T. Thole, "Molecular polarizabilities calculated with a modified dipole interaction," *Chem. Phys.* **59**, 341–350 (1981).
- ³³T. A. Halgren, "The representation of van der Waals (vdW) interactions in molecular mechanics force fields: Potential form, combination rules, and vdW parameters," *J. Am. Chem. Soc.* **114**, 7827–7843 (1992).
- ³⁴J. W. Ponder, C. Wu, P. Ren, V. S. Pande, J. D. Chodera, M. J. Schnieders, I. Haque, D. L. Mobley, D. S. Lambrecht, R. A. DiStasio, Jr. *et al.*, "Current status of the AMOEBA polarizable force field," *J. Phys. Chem. B* **114**, 2549–2564 (2010).
- ³⁵R. E. Duke, O. N. Starovoytov, J.-P. Piquemal, and G. A. Cisneros, "GEM*: A molecular electronic density-based force field for molecular dynamics simulations," *J. Chem. Theory Comput.* **10**, 1361–1365 (2014).
- ³⁶M. Frisch, G. Trucks, H. B. Schlegel, G. Scuseria, M. Robb, J. Cheeseman, G. Scalmani, V. Barone, B. Mennucci, G. e. Petersson *et al.* GAUSSIAN 09, Revision D4, Gaussian, Inc., 2009.
- ³⁷J. W. Ponder, TINKER, Software Tools for Molecular Design, version 7.0, 2015.
- ³⁸D. Case, T. Darden, T. Cheatham III, C. Simmerling, J. Wang, R. Duke, R. Luo, R. Walker, W. Zhang, K. Merz *et al.*, AMBER 12 (University of California, San Francisco, 2012), pp. 1–3.
- ³⁹T. A. Darden, D. York, and L. G. Pedersen, "Particle mesh Ewald: An Nlog(N) method for Ewald sums," *J. Chem. Phys.* **98**, 10089–10092 (1993).
- ⁴⁰U. Essmann, L. Perera, M. Berkowitz, T. A. Darden, H. Lee, and L. G. Pedersen, "A smooth particle mesh Ewald method," *J. Chem. Phys.* **103**, 8577–8593 (1995).
- ⁴¹K. Nam, J. Gao, and D. M. York, "An efficient linear-scaling Ewald method for long-range electrostatic interactions in combined QM/MM calculations," *J. Chem. Theory Comput.* **1**, 2–13 (2005).
- ⁴²C. Hardacre, J. D. Holbrey, S. J. McMath, D. T. Bowron, and A. K. Soper, "Structure of molten 1,3-dimethylimidazolium chloride using neutron diffraction," *J. Chem. Phys.* **118**, 273–278 (2003).
- ⁴³V. Chaban and J. Voroshilova, "Systematic refinement of Canongia Lopes-Pádua force field for pyrrolidinium-based ionic liquids," *J. Phys. Chem. B* **119**(20), 6242–6249 (2015).
- ⁴⁴J. B. Haskins, W. R. Bennett, J. J. Wu, D. M. Hernández, O. Borodin, J. D. Monk, C. W. Bauschlicher, Jr., and J. W. Lawson, "Computational and experimental investigation of Li-doped ionic liquid electrolytes: [pyr14][TFSI], [pyr13][FSI], and [EMIM][BF₄]," *J. Phys. Chem. B* **118**(38), 11295–11309 (2014).
- ⁴⁵Z.-B. Zhou, H. Matsumoto, and K. Tatsumi, "Cyclic quaternary ammonium ionic liquids with perfluoroalkyltrifluoroborates: Synthesis, characterization, and properties," *Chem. - Eur. J.* **12**, 2196–2212 (2006).
- ⁴⁶M. J. Monteiro, F. F. Bazito, L. J. Siqueira, M. C. Ribeiro, and R. M. Torresi, "Transport coefficients, Raman spectroscopy, and computer simulation of lithium salt solutions in an ionic liquid," *J. Phys. Chem. B* **112**, 2102–2109 (2008).
- ⁴⁷O. Borodin and G. D. Smith, "Quantum chemistry and molecular dynamics simulation study of dimethyl carbonate: Ethylene carbonate electrolytes doped with LiPF₆," *J. Phys. Chem. B* **113**, 1763–1776 (2009).
- ⁴⁸Z. Li, G. D. Smith, and D. Bedrov, "Li⁺ solvation and transport properties in ionic liquid/lithium salt mixtures: A molecular dynamics simulation study," *J. Phys. Chem. B* **116**, 12801–12809 (2012).
- ⁴⁹D. H. Zaitsev, A. V. Yermalayev, V. N. Emel'yanenko, A. Heintz, S. P. Verevkin, C. Schick, S. Berdzinski, and V. Strehmel, "Structure–property relationships in ILs: Vaporization enthalpies of pyrrolidinium based ionic liquids," *J. Mol. Liq.* **192**, 171–176 (2014).
- ⁵⁰K. Hayamizu, Y. Aihara, H. Nakagawa, T. Nukuda, and W. S. Price, "Ionic conduction and ion diffusion in binary room-temperature ionic liquids composed of [emim][BF₄] and LiBF₄," *J. Phys. Chem. B* **108**, 19527–19532 (2004).